

Article

Pressure Induced Superconductivity and Multiple Structural Transitions in CsCl-Type Cubic CeZn Single Crystal

Xiaoling Shen ^{1,*}, Hanming Ma ², Dilip Bhoi ² , Jun Gouchi ², Yoshiya Uwatoko ^{2,*}, Alisha Dalan ³, Yukihiro Kawamura ³, Hiroyasu Sato ⁴, Izuru Umehara ¹  and Masatomo Uehara ^{1,*} 

¹ Department of Physics, Yokohama National University, 79-1 Tokiwadai, Hodogaya-ku, Yokohama 240-8501, Japan; umehara-izuru-xn@ynu.ac.jp

² Institute for Solid State Physics, University of Tokyo, Kashiwa 277-8581, Japan; mhm@issp.u-tokyo.ac.jp (H.M.); dilipkbhoi@g.ecc.u-tokyo.ac.jp (D.B.); gouchijun@yahoo.co.jp (J.G.)

³ Graduate School of Engineering, Muroran Institute of Technology, Muroran 050-8585, Japan; 21043004@mmm.muroran-it.ac.jp (A.D.); y_kawamura@mmm.muroran-it.ac.jp (Y.K.)

⁴ Rigaku Corporation, Akishima 196-8666, Japan; h-sato@rigaku.co.jp

* Correspondence: shen-xiaoling-nr@ynu.jp (X.S.); uwatoko@issp.u-tokyo.ac.jp (Y.U.); uehara-masatomo-cf@ynu.ac.jp (M.U.)

Abstract: CsCl-type cubic compound CeZn exhibits a paramagnetic (PM) to antiferromagnetic (AFM) first-order transition at $T_N \sim 30$ K accompanied by a simultaneous structural transition from cubic to tetragonal structure as temperature decreases. Applying the pressure, the coupled magnetic and crystal structural transition becomes separated above 1.0 GPa and then the AFM order changes to ferromagnetic (FM). The FM ordering temperature decreases with further applying pressure and changes to a nonmagnetic state above ~ 3.0 GPa. In the nonmagnetic state, we discovered superconductivity below $T_{sc} \sim 1.3$ K over 5.5 GPa, which survives even up to 9.5 GPa. Investigation of single crystal X-ray diffraction at room temperature reveals that CeZn undergoes a sequential crystal structural change with increasing pressure from cubic at ambient pressure to the monoclinic structure at 8.2 GPa via tetragonal and orthorhombic structure. The detailed analysis of crystal structure in CeZn single crystal evidenced that the emergence of superconductivity is related to the orthorhombic-to-monoclinic transition implying a nonmagnetic origin of the Cooper pair formation.

Keywords: CeZn; superconductor; high pressure; crystal structure



Citation: Shen, X.; Ma, H.; Bhoi, D.; Gouchi, J.; Uwatoko, Y.; Dalan, A.; Kawamura, Y.; Sato, H.; Umehara, I.; Uehara, M. Pressure Induced Superconductivity and Multiple Structural Transitions in CsCl-Type Cubic CeZn Single Crystal. *Crystals* **2022**, *12*, 571. <https://doi.org/10.3390/cryst12050571>

Academic Editors: Peng Deng, Huimin Zhang and Kwang-Yong Choi

Received: 30 March 2022

Accepted: 19 April 2022

Published: 20 April 2022

Publisher's Note: MDPI stays neutral with regard to jurisdictional claims in published maps and institutional affiliations.



Copyright: © 2022 by the authors. Licensee MDPI, Basel, Switzerland. This article is an open access article distributed under the terms and conditions of the Creative Commons Attribution (CC BY) license (<https://creativecommons.org/licenses/by/4.0/>).

1. Introduction

The CsCl-type compound crystallizing in cubic structure with chemical formula $ReTm$ (where Re = rare earth elements such as La, Ce, Pr ... etc., and Tm = transition metal elements such as Ag, Zn, Cd, ... etc.) have been known for last three decades due to their strong correlation between charge, spin, and lattice degrees of freedom [1–6]. These compounds undergo a cubic-to-tetragonal structural transition on cooling, followed by a magnetically ordered state at a lower temperature, like CeAg [1], PrAg [5]. The cubic-to-tetragonal structural transition in these compounds is known to originate from the band Jahn-Teller distortion [7,8]. Usually, the band Jahn-Teller effect in these compounds removes the degeneracy of $5d$ -orbitals of Re elements by a lattice deformation. As a result, the density of states near the Fermi level is expected to spread out in the tetragonal structure, thus repopulating the various sub-bands and effectively lowering the total energy. Remarkably, these transitions are very sensitive to external perturbation, thus revealing other emergent structures with varying tuning parameters such as chemical doping or pressure.

Among these, CeZn is distinct because the magnetic and crystal structural transitions are coupled, revealing a first-order nature of the transition [9–12]. CeZn exhibits AFM order below the Néel temperature, $T_N \sim 30$ K, and a concurrent crystal structural change from cubic to tetragonal structure [12]. So far, the electrical, magnetic, and structural properties

of CeZn have been investigated by substituting Cu in place of Zn, $\text{CeZn}_{1-x}\text{Cu}_x$, [13,14] and applying pressure up to 2.9 GPa [9]. The magnetic and structural transition temperature decreases with Cu substitution and stays coupled up to $x = 0.3$. With further Cu substitution, magnetic order changes from AFM to FM at $x = 0.6$ via a coexisting AFM and FM order region. For $x > 0.3$, $\text{CeZn}_{1-x}\text{Cu}_x$ reveals multiple structural changes with decreasing temperature [14]. On the other hand, the hydrostatic pressure studies on CeZn have shown that the magnetic and crystal structural transitions become separated above 1.0 GPa. The AFM order changes to FM, though, the neutron diffraction study pointed that the structure altered from cubic to rhombohedral structure in the FM state [12], different from the Cu substitution [14]. Moreover, the Curie temperature, T_C , of the FM state was found to decrease with pressure, while the crystal structural transition temperature increases and reaches to room temperature around 3.0 GPa [9,15]. Further investigation of the electronic and magnetic properties of CeZn at higher pressure is still unexplored.

In this study, we have extended the investigation of the electrical and structural properties of CeZn single crystal up to 9.5 GPa and down to 30 mK. Single crystal X-ray diffraction of CeZn under pressure revealed that the previously assumed rhombohedral structure above 1.0 GPa to be the tetragonal structure. In addition, we detect two more crystal structural transitions: one to an orthorhombic structure at 4.2 GPa and another to a monoclinic structure at 8.2 GPa. Interestingly, in the vicinity of the latter crystal structural transition, we also discovered that CeZn becomes superconductor below $T_{sc} \sim 1.3$ K persisting up to 9.5 GPa.

2. Single Crystal Growth and Experimental Technique

CeZn single crystals were synthesized by melting Ce and Zn with a 1:1 ratio as starting materials in a tungsten crucible sealed inside a quartz tube under vacuum. The mixture was heated to 1000 °C in 10 h and cooled down to 900 °C in 3 h. Then the mixture was slowly cooled to 820 °C in 10 days and subsequently quenched to room temperature. Silver color CeZn single crystals were collected mechanically from the tungsten crucible. The residual resistivity ratio ($RRR \sim 20$) of the obtained sample reflects the high quality of the single crystals.

Resistivity under high pressure was measured using a clamp type piston cylinder cell and a palm cubic anvil cell (PCAC). For pressure up to 2.5 GPa, we used Daphne 7373 as pressure transmitting medium in clamp-type piston cylinder cell, whereas Fluorinert FC70:FC77 (1:1) was used as the pressure transmitting medium for measurements above 2.5 GPa in PCAC. Note that, the PCAC is well known for generating hydrostatic pressure due to the multiple anvil geometry [16,17] pressure up to 15 GPa, though the Fluorinert FC70:FC77 (1:1) is solidified at about 2.3 GPa [18,19]. The electrical resistivity down to 30 mK was measured in a Bluefors-LD400 cryogen-free dilution refrigerator system. High pressure single crystal X-ray diffraction experiments at room temperature were performed by using a diamond anvil cell (DAC). The sample was compressed inside the Rhenium gaskets, which had a 160- μm diameter hole, placed in the DAC. The mixture of methanol and ethanol alcohol (4:1) was used as pressure transmitting medium. The pressure was determined by the ruby fluorescence technique at room temperature [20]. The single crystal X-ray diffraction was carried out by using Rigaku XtaLab HyPix-6000 diffractometer with Mo- $K\alpha$ radiation ($\lambda = 0.71073$ Å). The single-crystal X-ray diffraction data have been processed using empirical absorption correction using the CrysAlis Pro program. The structure was solved by direct methods with the ShelXT [21] and refined using the ShelXL [22] programs as a part of the Olex2 software package [23].

3. Results and Discussion

3.1. Electrical Resistivity under Pressure

Figure 1a shows the temperature dependence of the electrical resistivity ρ of a CeZn single crystal at some selected pressures from 300 K down to 30 mK. At ambient pressure, $\rho(T)$ monotonically decreases with temperature and drops suddenly below $T_N = 29.0$ K. It is clear from Figure 1a that the coupled structural and magnetic transition become separated

on increasing pressure above 1.0 GPa, in agreement with the earlier report [9,12]. At 1.3 GPa, the bend at the lower temperature side is assigned to the pressure-induced FM state, while the thermal hysteresis appearing at the high temperature side is attributed to the crystal structural transition. On increasing pressure to 2.0 GPa, FM state shifts towards lower temperature and the crystal structural transition temperature almost reaches to 280 K. Here, it is worthy to note that, in contrast to earlier result [9], in the present case, the crystal structural transition exceeds room temperature at lower pressure. This is clear by the absence of hysteretic behavior in $\rho(T)$ below 300 K even at 2.9 GPa. This difference is attributed to the higher quality of sample used in the present study than the earlier polycrystalline samples [9]. Moreover, at 2.9 GPa, the signature of T_C disappears, and another big hump appears around 100 K, implying the pronounced Kondo effect. Up to 5.0 GPa, $\rho(T)$ shows a normal metallic behavior in the measured temperature range. Surprisingly, on slightly increasing the pressure to 5.5 GPa as shown in Figure 1b, $\rho(T)$ displays a pronounced drop below ~ 1.3 K and reaches zero around 0.8 K, signaling the occurrence of a superconducting state. At higher pressure, the transition into the superconducting state becomes sharper. We also confirmed the signature of bulk superconductivity above 5.5 GPa using the ac magnetic susceptibility.

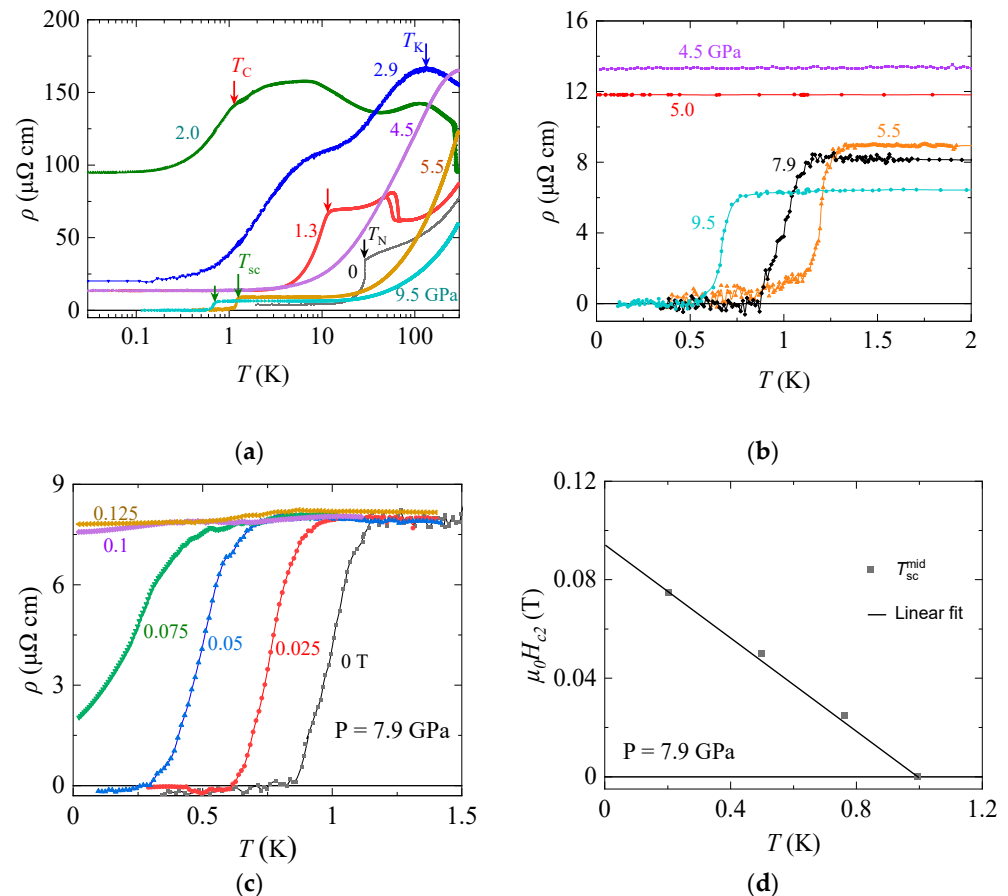


Figure 1. (a) Temperature dependence of electrical resistivity ρ , of CeZn single crystal at some selected pressures. Black and red arrows show the magnetic transition temperatures, T_N and T_C , respectively. Blue arrow indicates Kondo temperature (T_K), and green arrows indicate superconductivity transition temperature (T_{sc}); (b) A zoomed-in view of the low temperature $\rho(T)$ for pressure above 4.5 GPa displaying the superconducting transitions. (c) $\rho(T)$ near the superconducting transition under different applied magnetic fields at 7.9 GPa. (d) Temperature dependence of upper critical field $\mu_0 H_{c2}$ estimated from the T_{sc}^{mid} as described in the main text.

To extract further insights into the nature of the superconducting state, we measured the temperature dependence of ρ near the superconducting region at the different fixed

magnetic fields as shown in Figure 1c for 7.9 GPa. With increasing magnetic field, the superconducting transition shifts towards lower temperature and the superconducting state is completely suppressed at 0.125 T. In Figure 1d, we plot the temperature dependence of the upper critical field $\mu_0 H_{c2}(T)$ estimated from the mid-point of the superconducting transition, T_{sc}^{mid} , at different magnetic fields. At a particular field, T_{sc}^{mid} is defined as the temperature where the resistivity drops to the half of normal state resistivity value. $\mu_0 H_{c2}(T)$ is described by a linear fitting, which yields a $\mu_0 H_{c2}(0) = 0.095$ T. We estimate the coherence length $\xi = 579$ Å, using the Ginzburg-Landau relationship: $\mu_0 H_{c2}(0) = \Phi_0 / 2\pi\xi^2$, where $\Phi_0 = 2.067 \times 10^{-15}$ Wb is the magnetic flux quantum. The small $\mu_0 H_{c2}(0)$ points that the superconducting state in CeZn does not arise from the unconventional mechanism of cooper pairing like in typical heavy fermion superconductors [24,25].

3.2. Crystal Structural Transition under Pressure

Earlier crystal structure investigation of CeZn under pressure [15], detected a structural transition around 2.6 GPa at room temperature. The signature of this structural transition is also reflected in the $\rho(T)$ curves measured at different pressure points as shown in Figure 1a. Therefore, to obtain preliminary information regarding the critical pressure, close to where the structural transitions may occur, we measured the resistivity of CeZn single crystal with varying pressure at $T = 300$ K, as shown in Figure 2. The $\rho(P)$ reveals a nonmonotonic behavior as a function of pressure. At 2.1 GPa, $\rho(P)$ rises rapidly suggesting the crystal structural transition, in agreement with a previous report [15]. The resistivity attains a maximum value of 4.0 GPa followed by a sudden drop around 5.2 GPa. Besides, a shoulder like feature can be seen at 7.9 GPa, which becomes clearer from the pressure dependence of $d\rho/dP$.

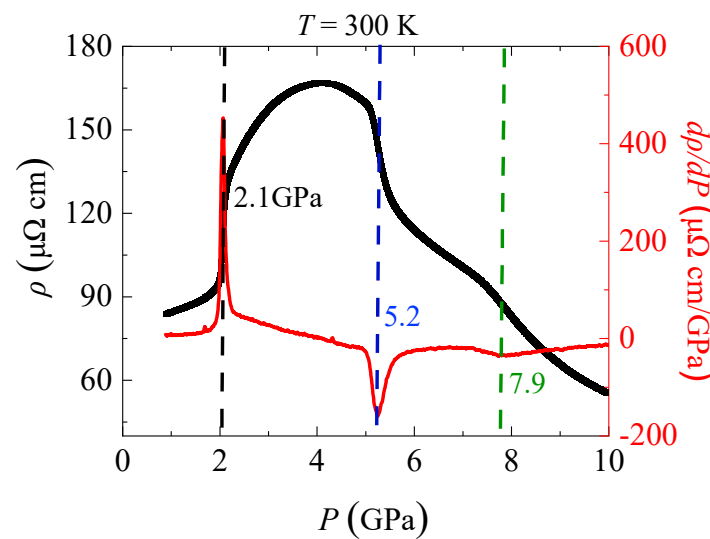


Figure 2. Pressure dependence of, ρ , of CeZn single crystal at $T = 300$ K (black line) and the derivatives $d\rho/dP$ (red line).

To find the microscopic origin of these anomalies, we performed single crystal X-ray diffraction of CeZn at selected pressures very close to the anomalies seen in $d\rho/dP$. The details of the crystallographic parameters obtained from the analysis of single crystal X-ray diffraction results at 0, 2.8 GPa, 4.2 GPa and 8.2 GPa are presented in Table 1. From the X-ray diffraction analysis, we deduce that the crystal structure of CeZn sequentially evolves with increasing pressure from a cubic structure (at ambient pressure) to tetragonal (at 2.8 GPa), orthorhombic (at 4.2 GPa) and finally to monoclinic (at 8.2 GPa). The crystallographic unit cell parameters were determined from 1143 measured reflections at ambient pressure. The estimated a -axis lattice parameter, 3.7034 (10) Å with space group $Pm\bar{3}m$ is consistent with earlier results [10]. Moreover, in this cubic structure, each Ce atom is surrounded by eight Zn atoms, forming a body-centered cube as shown in Figure 3a.

Table 1. Crystallographic parameters of CeZn single crystal at some selected pressures.

| Pressure (GPa) | 0 | 2.8 | 4.2 | 8.2 |
|---------------------------------------|--------------|------------|--------------|------------|
| Crystal System | Cubic | Tetragonal | Orthorhombic | Monoclinic |
| Space Group | $Pm\bar{3}m$ | $P4/nmm$ | $Pma2$ | $P2_1/m$ |
| $a/\text{\AA}$ | 3.7034(10) | 5.113(2) | 4.966(13) | 6.190(3) |
| $b/\text{\AA}$ | 3.7034(10) | 5.113(2) | 5.157(6) | 4.659(7) |
| $c/\text{\AA}$ | 3.7034(10) | 3.623(12) | 3.548(19) | 6.200(5) |
| $\alpha/^\circ$ | 90 | 90 | 90 | 90 |
| $\beta/^\circ$ | 90 | 90 | 90 | 113.66(8) |
| $\gamma/^\circ$ | 90 | 90 | 90 | 90 |
| $V/\text{\AA}^3$ | 50.793(4) | 94.7(3) | 90.8(3) | 163.8(3) |
| D ($\text{g}\cdot\text{cm}^{-3}$) | 6.718 | 7.207 | 7.512 | 8.334 |
| Z | 1 | 2 | 2 | 4 |
| Measured Refl. | 1143 | 398 | 311 | 559 |
| Independent Refl. | 33 | 37 | 103 | 143 |
| Reflections with $I > 2(I)$ | 33 | 35 | 88 | 116 |
| R_{int} (%) | 5.51 | 9.64 | 4.49 | 7.36 |
| Goof | 1.107 | 1.312 | 1.285 | 1.330 |

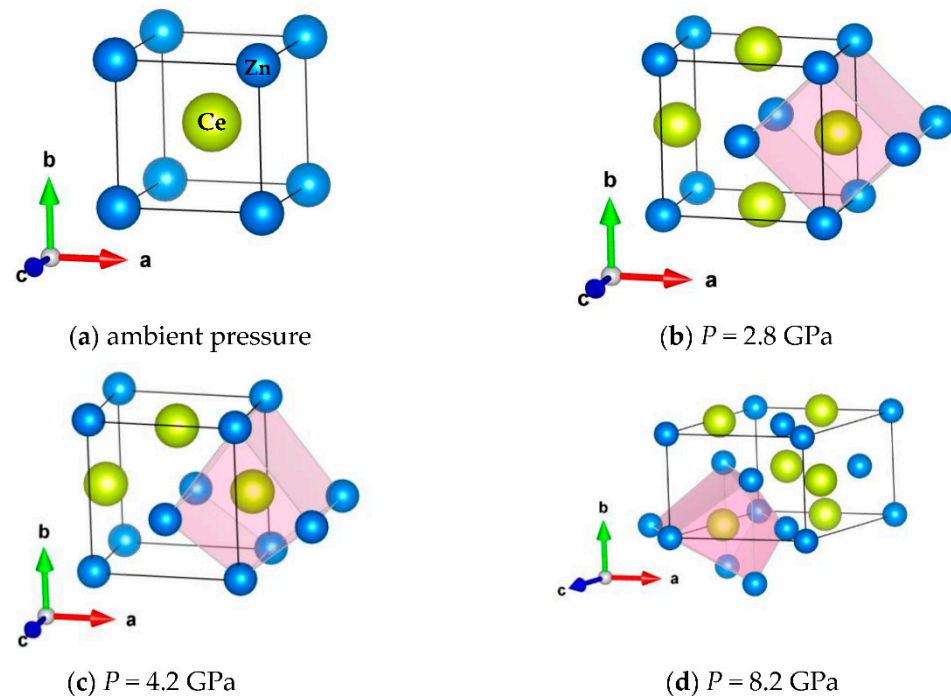


Figure 3. The crystal structure of the CeZn at some selected pressures. (a) Cubic structure at ambient pressure; (b) tetragonal structure at 2.8 GPa; (c) orthorhombic structure at 4.2 GPa; (d) monoclinic structure at 8.2 GPa. The pink outline shows the gradual distortion of the cube consisting of a Ce atom at the body-centered position surrounded by eight Zn atoms with increasing pressure.

At 2.8 GPa, the present X-ray diffraction results indicate that cubic structure changes to the tetragonal structure (space group: $P4/nmm$) as shown in Figure 3b, rather than the rhombohedral structure obtained by neutron diffraction [12]. We attribute these different results to the high precision measurement of single crystal X-ray diffraction in the present experiment as well as analysis of the data by considering 398 measured reflections compared to the analysis of a single peak in neutron diffraction study. In this tetragonal structure, the lattice parameter in the ab plane expands by $\sqrt{2}$ times the lattice constant at ambient pressure, doubling the chemical formula unit, Z , per unit cell. The estimated lattice parameters are $a = b = 5.113(2)$ \AA and $c = 3.623(12)$ \AA . This newly assigned tetragonal structure in the FM phase of CeZn, put CeZn in the same class with other CsCl-type

rare earth compounds like CeAg [1], CeCd [4], and PrAg [5], which undergo a cubic to tetragonal structural transition under pressure.

At 4.2 GPa, from analysis of 311 measured reflections, we identify that CeZn transition into an orthorhombic structure with space group $Pma2$ as shown in Figure 3c. Surprisingly, near this crystal structural transition, $\rho(P)$ does not display any anomaly. In orthorhombic structure, the b -axis unit cell parameter elongates while the a -axis, as well as the c -axis shrink, compared to the tetragonal unit cell. With further compression to 8.2 GPa, the orthorhombic structure changes to the monoclinic structure (space group $P2_1/m$) as shown in Figure 3d, accompanied by an increase in the number of chemical formula units Z , from 2 to 4. In Figure 2, the sudden drop in ρ around 5.2 GPa indicates that near this pressure possibly the crystal structure started to change from orthorhombic to monoclinic structure. Moreover, very close to this pressure the nonmagnetic state of CeZn changes to a superconducting state at low temperature. COD numbers 3000358 (cubic structure), 3000359 (tetragonal structure), 3000360 (orthorhombic structure), 3000361 (monoclinic structure) contain the supplementary crystallographic data for this paper. These data can be obtained free of charge via <http://www.crystallography.net/cod/search.html> (accessed on 1 March 2022).

From the analysis of the single crystal XRD pattern of CeZn, we obtained crucial insights into the local atomic arrangements of CeZn. At ambient pressure, each Ce atom is surrounded by eight Zn atoms, forming a body-centered cube. At higher pressure, the periodic arrangement of Ce and Zn atoms in the tetragonal, orthorhombic, and monoclinic structure can be represented by a distorted body centered cubic lattice. With increasing pressure, the cube becomes more distorted and lowers the overall crystal structural symmetry of CeZn. Remarkably, after releasing the pressure slowly, the structure reverts to the parent cubic structure at ambient pressure.

3.3. Pressure-Temperature Phase Diagram

From the structural study at room temperature, it is clear that CeZn undergoes multiple crystal structural transitions with pressure variation. To find a correlation between the crystal structure and the underlying electronic properties with increasing pressure, we have constructed a temperature (T)—pressure (P) phase diagram of CeZn, as shown in Figure 4. At room temperature, CeZn undergoes multiple crystal structural transitions with increasing pressure from cubic at ambient pressure to the monoclinic structure at 8.2 GPa via tetragonal (at 2.8 GPa) and orthorhombic structure (at 4.2 GPa). The coupled magnetic transition, PM to AFM state, and the structural transition, cubic to tetragonal structure due to the magnetic striction, at T_N decreases hardly up to 1.0 GPa [9,10,12]. Above 1.0 GPa, the pressure induced another cubic-to-tetragonal structural transition caused by the band Jahn-Teller effect [7,8]. The crystal structural transition temperature systematically increases with applying pressure, as evidenced by the hysteresis in $\rho(T)$ moving towards room temperature [9]. However, whether the other two crystal structural transition temperatures vary with applied pressure is not clear. The T - P phase diagram reveals that the electronic properties of CeZn also change simultaneously across the structural transitions. First, the ground state changes AFM to FM due to the cubic-to-tetragonal structural transition with pressure. T_C decreases rapidly to 1.1 K in the tetragonal structure as pressure increases to 2.0 GPa, implying a possible existence of a quantum critical point, different from the results in Ref. [9]. Secondly, at the tetragonal-to-orthorhombic structural transition, CeZn transforms into a nonmagnetic simple metallic state. Finally, superconductivity emerges below $T_{sc} \sim 1.3$ K around 5.5 GPa possibly when the crystal structure changes from orthorhombic to monoclinic. The superconducting states survive up to 9.5 GPa in the monoclinic crystal structure. Here, it is worth noting that the T - P diagram of CeZn is different from that of the other Ce-based superconductors, such as CePd₂Si₂ [26,27], CeIn₃ [28,29], CeRhIn₅ [30] and CeCu₂Si₂ [31]. In these cases, superconductivity appears very close to the magnetic quantum critical point, whereas superconductivity in CeZn appears far away from the magnetic state. These results may suggest that the emergence of superconductivity in CeZn

under pressure is related to the change in crystal structure implying a nonmagnetic origin of the Cooper pair formation, which is well supported by a rather small $H_{c2}(0) \sim 0.095$ T.

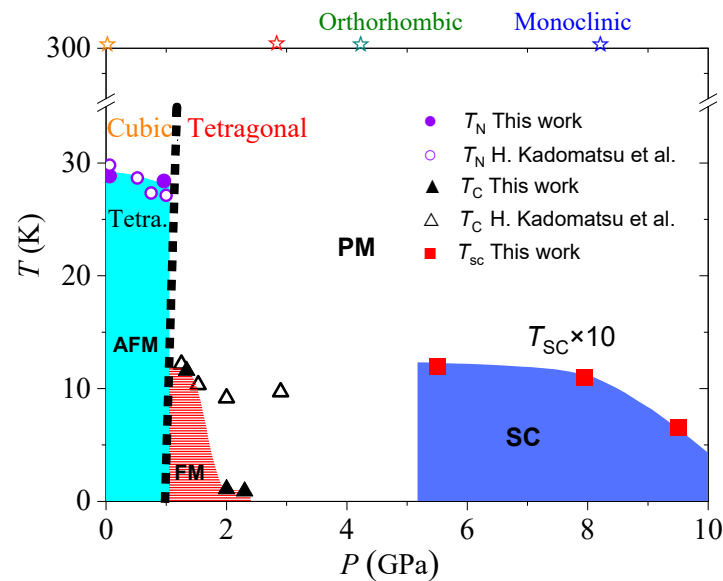


Figure 4. Temperature-pressure phase diagram of CeZn. T_N , T_C , and T_{sc} are the Néel temperature, the Curie temperature and the superconducting transition temperature determined from the resistivity data, respectively. For clarity, T_{sc} has been multiplied by a factor of 10. The stars indicate the pressure value at which the single crystal X-ray diffraction measurements are performed. The tetragonal structure in the AFM region is obtained from Refs. [10,12]. The cubic to the tetragonal structure boundary line has been used from Ref. [9].

In summary, we have performed systematic electrical resistivity and single crystal X-ray diffraction measurement of CeZn under high pressure up to 9.5 GPa. We find that CeZn exhibits multiple crystal structural transitions under pressure. Simultaneously, across these crystal structural transitions, the signature of modification of the underlying electronic properties of CeZn is also detected. The pressure induced cubic-to-tetragonal transition results in the AFM-to-FM change. With further pressure increases, the orthorhombic structure appears in nonmagnetic phase. In addition, we observed a superconducting state near the orthorhombic-to-monoclinic structural change of CeZn with a small $H_{c2}(0) \sim 0.095$ T suggesting that nonmagnetic nature of the cooper pair formation. Also, we would like to add that further investigation of how crystal structural change with decreasing temperature at a fixed pressure is required for detailed understanding about the relationship between the crystal structure and electronic properties.

Author Contributions: Conceptualization, X.S.; formal analysis, X.S., D.B., Y.U., I.U. and M.U.; investigation, X.S., H.M. and J.G.; writing—original draft preparation, X.S.; writing—review and editing, X.S., H.M., D.B., J.G., Y.U., A.D., Y.K., H.S., I.U. and M.U.; supervision, Y.U., I.U. and M.U.; project administration, X.S., Y.U.; funding acquisition, Y.U. All authors have read and agreed to the published version of the manuscript.

Funding: This research was funded by JSPS KAKENHI Grant Numbers JP19H00648.

Institutional Review Board Statement: Not applicable.

Informed Consent Statement: Not applicable.

Data Availability Statement: Not applicable.

Acknowledgments: We are thankful to S. Nagasaki for technical help during the experiments.

Conflicts of Interest: The authors declare no conflict of interest. The funders had no role in the design of the study; in the collection, analyses, or interpretation of data; in the writing of the manuscript, or in the decision to publish the results.

References

1. Kurisu, M.; Kadomatsu, H.; Fujiwara, H. Magnetic and structural properties of CeAg at high pressure. *J. Phys. Soc. Jpn.* **1983**, *52*, 4349–4355. [[CrossRef](#)]
2. Cornelius, A.L.; Gangopadhyay, A.K.; Schilling, J.S.; Assmus, W. Hydrostatic high-pressure studies on the ferromagnetic Kondo-lattice compounds CePdSb and CeAg to 16 GPa. *Phys. Rev. B* **1997**, *55*, 14109. [[CrossRef](#)]
3. Kurisu, M.; Tanaka, H.; Kadomatsu, H.; Sekizawa, K.; Fujiwara, H. Magnetic and Structural Properties of CeTi at Hydrostatic Pressure. *J. Phys. Soc. Jpn.* **1985**, *54*, 3548–3553. [[CrossRef](#)]
4. Kadomatsu, H.; Kurisu, M.; Kitai, T.; Okamoto, T.; Fujiwara, H. Magnetic and structural phase transition of CeCd at hydrostatic pressure. *Phys. Lett. A* **1983**, *94*, 178–180. [[CrossRef](#)]
5. Kadomatsu, H.; Kurisu, M.; Fujiwara, H. Magnetic and structural properties of PrAg at high pressure. *J. Phys. Soc. Jpn.* **1984**, *53*, 1819–1827. [[CrossRef](#)]
6. Peukert, H.; Schilling, J.S. Effect of hydrostatic pressure on phase transition and superconductivity in $\text{LaAg}_x\text{In}_{1-x}$, LaCd and LaZn. *Z. Für Phys. B Condens. Matter* **1981**, *41*, 217–222. [[CrossRef](#)]
7. Ihrig, H.; Vigren, D.T.; Kübler, J.; Methfessel, S. Cubic-to-Tetragonal Transformation and Susceptibility in $\text{LaAg}_x\text{In}_{1-x}$ Alloys. *Phys. Rev. B* **1973**, *8*, 4525. [[CrossRef](#)]
8. Asano, S.; Ishida, S. Band Jahn-Teller Effect in LaCd. *J. Phys. Soc. Jpn.* **1985**, *54*, 4241–4245. [[CrossRef](#)]
9. Kadomatsu, H.; Tanaka, H.; Kurisu, M.; Fujiwara, H. Kondo state and pressure-induced ferromagnetism in CeZn. *Phys. Rev. B* **1986**, *33*, 4799. [[CrossRef](#)]
10. Schmitt, D.; Morin, P.; Pierre, J. Magnetic structure and crystal field in cerium compounds with CsCl-type structure. *J. Magn. Magn. Mater.* **1978**, *8*, 249–256. [[CrossRef](#)]
11. Pierre, J.; Murani, A.P.; Galera, R.M. Magnetic susceptibility, electrical resistivity and neutron spectroscopy of some cubic cerium intermetallics. *J. Phys. F Met. Phys.* **1981**, *11*, 679. [[CrossRef](#)]
12. Shigeoka, T.; Uwatoko, Y.; Fujii, H.; Rebelsky, L.; Shapiro, S.M.; Asai, K. Pressure-induced structural and magnetic phase transitions in CeZn. *Phys. Rev. B* **1990**, *42*, 8394. [[CrossRef](#)] [[PubMed](#)]
13. Uwatoko, Y.; Fujii, H.; Nishi, M.; Motoya, K.; Ito, Y. Neutron diffraction and magnetic studies of $\text{CeZn}_{1-x}\text{Cu}_x$ single crystals. *J. Magn. Magn. Mater.* **1988**, *76*, 411–412. [[CrossRef](#)]
14. Uwatoko, Y.; Fujii, H.; Nishi, M.; Motoya, K.; Ito, Y. A new crystallographic phase transition in the CsCl-type $\text{CeZn}_{1-x}\text{Cu}_x$ compounds. *Solid State Commun.* **1989**, *72*, 941–943. [[CrossRef](#)]
15. Uwatoko, Y.; Suenaga, K.; Oomi, G. X-ray diffraction study of the structural change in CeZn under high pressure. *J. Magn. Magn. Mater.* **1992**, *104*, 645–646. [[CrossRef](#)]
16. Cheng, J.G.; Matsubayashi, K.; Nagasaki, S.; Hisada, A.; Hirayama, T.; Hedo, M.; Uwatoko, Y. Integrated-fin gasket for palm cubic-anvil high pressure apparatus. *Rev. Sci. Instrum.* **2014**, *85*, 093907. [[CrossRef](#)]
17. Mori, N.; Takahashi, H.; Takeshita, N. Low-temperature and high-pressure apparatus developed at ISSP, University of Tokyo. *High Press. Res.* **2004**, *24*, 225–232. [[CrossRef](#)]
18. Sidorov, V.A.; Sadykov, R.A. Hydrostatic limits of Fluorinert liquids used for neutron and transport studies at high pressure. *J. Phys. Condens. Matter* **2005**, *17*, S3005. [[CrossRef](#)]
19. Torikachvili, M.S.; Kim, S.K.; Colombier, E.; Bud'Ko, S.L.; Canfield, P.C. Solidification and loss of hydrostaticity in liquid media used for pressure measurements. *Rev. Sci. Instrum.* **2015**, *86*, 123904. [[CrossRef](#)]
20. Mao, H.K.; Xu, J.A.; Bell, P.M. Calibration of the ruby pressure gauge to 800 kbar under quasi-hydrostatic conditions. *J. Geophys. Res. Solid Earth* **1986**, *91*, 4673–4676. [[CrossRef](#)]
21. Sheldrick, G.M. SHELXT—Integrated space-group and crystal-structure determination. *Acta Crystallogr. Sect. A Found. Adv.* **2015**, *71*, 3–8. [[CrossRef](#)] [[PubMed](#)]
22. Sheldrick, G.M. Crystal structure refinement with SHELXL. *Acta Crystallogr. Sect. C Struct. Chem.* **2015**, *71*, 3–8. [[CrossRef](#)] [[PubMed](#)]
23. Dolomanov, O.V.; Bourhis, L.J.; Gildea, R.J.; Howard, J.A.; Puschmann, H. OLEX2: A complete structure solution, refinement and analysis program. *J. Appl. Crystallogr.* **2009**, *42*, 339–341. [[CrossRef](#)]
24. Jaccard, D.; Behnia, K.; Sierro, J. Pressure induced heavy fermion superconductivity of CeCu_2Ge_2 . *Phys. Lett. A* **1992**, *163*, 475–480. [[CrossRef](#)]
25. Vargoz, E.; Jaccard, D.; Genoud, J.Y.; Brison, J.P.; Flouquet, J. Upper critical field of CeCu_2Si_2 at very high pressure. *Solid State Commun.* **1998**, *106*, 631–636. [[CrossRef](#)]
26. Grosche, F.M.; Walker, I.R.; Julian, S.R.; Mathur, N.D.; Freye, D.M.; Steiner, M.J.; Lonzarich, G.G. Superconductivity on the threshold of magnetism in CePd_2Si_2 and CeIn_3 . *J. Phys. Condens. Matter* **2001**, *13*, 2845. [[CrossRef](#)]
27. Demuer, A.; Jaccard, D.; Sheikin, I.; Raymond, S.; Salce, B.; Thomasson, J.; Flouquet, J. Further pressure studies around the magnetic instability of CePd_2Si_2 . *J. Phys. Condens. Matter* **2001**, *13*, 9335. [[CrossRef](#)]

28. Walker, I.R.; Grosche, F.M.; Freye, D.M.; Lonzarich, G.G. The normal and superconducting states of CeIn₃ near the border of antiferromagnetic order. *Phys. C Supercond.* **1997**, *282*, 303–306. [[CrossRef](#)]
29. Knebel, G.; Braithwaite, D.; Canfield, P.C.; Lapertot, G.; Flouquet, J. Electronic properties of CeIn₃ under high pressure near the quantum critical point. *Phys. Rev. B* **2001**, *65*, 024425. [[CrossRef](#)]
30. Hegger, H.; Petrovic, C.; Moshopoulou, E.G.; Hundley, M.F.; Sarrao, J.L.; Fisk, Z.; Thompson, J.D. Pressure-induced superconductivity in quasi-2D CeRhIn₅. *Phys. Rev. Lett.* **2000**, *84*, 4986. [[CrossRef](#)]
31. Rueff, J.P.; Raymond, S.; Taguchi, M.; Sikora, M.; Itié, J.P.; Baudalet, F.; Jaccard, D. Pressure-induced valence crossover in superconducting CeCu₂Si₂. *Phys. Rev. Lett.* **2011**, *106*, 186405. [[CrossRef](#)] [[PubMed](#)]